

PACS numbers: 42.55.Ye; 42.60.Lh; 42.81.Cn; 42.81.Dp
DOI: 10.1070/QE2015v045n09ABEH015881

Efficient 1.9-μm Raman generation in a hydrogen-filled hollow-core fibre

A.V. Gladyshev, A.N. Kolyadin, A.F. Kosolapov, Yu.P. Yatsenko,
A.D. Pryamikov, A.S. Biriukov, I.A. Bufetov, E.M. Dianov

Abstract. **Efficient Raman generation in a molecular hydrogen-filled hollow-core fibre having a cladding in the form of a single ring of capillaries has been demonstrated for the first time. The pump source used was a *Q*-switched Nd:YAG laser with a pulse duration of 125 ns, and a single-pass (cavity-free) configuration was employed. The maximum average output power at 1.9 μm was 300 mW, and the differential quantum efficiency was 87%, a record level for such experiments.**

Keywords: *Raman lasers, hollow-core fibres, fibre lasers.*

1. Introduction

Raman lasers (or SRS lasers) are currently among the most efficient frequency conversion devices. The quantum efficiency of both fibre [1] and solid-state [2] Raman lasers reaches tens of percent, approaching unity in a number of cases. Whereas a typical frequency shift Ω in solids is $\sim$100 cm^{-1}, Raman lasers that employ hydrogen, the lightest gas, ensure a frequency shift $\Omega = 4155$ cm^{-1} owing to a stimulated vibrational Raman transition in molecular hydrogen [3]. As shown in experiments with hydrogen-filled cells, single- and two-stage hydrogen Raman lasers ensure highly efficient long-wavelength generation in the ranges 1.87–1.9 and 8–9 μm [4], as well as in the 16 μm range [5] and even near 30 μm [6]. However, in the case of usual pump beam focusing into a gas cell by lenses, pump powers on the order of megawatts or higher were needed to reach Raman threshold. The use of waveguide structures allows one to considerably increase the interaction length of pump light in a Raman-active medium, ensuring a considerable reduction in threshold pump intensity and power. Even the first experiments aimed at creating Raman lasers based on silica glass fibre [7, 8] demonstrated the possibility of lasing at pump powers under 100 W. The use of silica glass fibres with almost lowest possible optical losses and fibre Bragg gratings as mirrors made it possible to produce efficient multistage Raman fibre lasers [9].

The Raman shift in silica glass fibres does not exceed 1330 cm^{-1} (Raman amplification at this frequency shift is observed in phosphosilicate glass fibres [10]). The shift is far smaller than that in hydrogen Raman lasers, and increasing the number of conversion stages to compensate for the small shift reduces the efficiency of the Raman laser [11], even with no allowance for the increase in the optical loss in the fibre at long wavelengths of the IR spectral region (see e.g. Dianov et al. [12]). The advent of hollow-core (HC) fibres with comparatively low losses [13] paved the way to gas-filled fibre lasers, including those based on stimulated Raman scattering (SRS). In particular, hydrogen-filled hollow-core fibres were successfully used to make highly efficient pulsed Raman fibre lasers employing vibrational and rotational transitions of molecular hydrogen [14–16]. Moreover, Couny et al. [17] demonstrated a cw Raman fibre laser employing a rotational transition of ortho-hydrogen, with a frequency shift $\omega = 587$ cm^{-1} (conversion of pump light at a wavelength $\lambda_p = 1064$ nm to Stokes-shifted light at $\lambda_S = 1135$ nm). Very recently, Wang et al. [18] have for the first time demonstrated efficient (48% quantum efficiency) Raman conversion from $\lambda_p = 1.06$ μm to $\lambda_S = 1.9$ μm in a hydrogen-filled hollow-core fibre. An essential point is that their Raman laser operated in pulsed (pulse duration $\tau = 0.7$ ns), transient (in terms of phase relaxation) mode, which prevented it from reaching the largest possible Raman gain coefficient [18].

Various cladding designs have been proposed for hydrogen Raman fibre lasers. Use was made first of Kagome lattice photonic crystal fibres (PCFs) [14] (Fig. 1a) and then of PCFs with a hexagonal reflective cladding structure [16] (Fig. 1b). In searching for a hollow-core fibre cladding configuration minimising the optical loss, Wang et al. [19, 20] proposed fibres with a hypocycloid-shaped core–cladding interface (Fig. 1c), and Pryamikov et al. [21] proposed fibres with a simple structure, whose cladding had the form of a single ring of capillaries (which were referred to as fibres with a negative curvature of the core–cladding interface) (Fig. 1d). Subsequently, this term was applied not only to fibres with a hypocycloid-shaped core but also to later proposed fibres whose cladding consisted of elements resembling a stylised image of a parachute [22] (Fig. 1e). But fibres of the type proposed by Pryamikov et al. [21] (Fig. 1d) differ significantly from other fibres with a negative curvature of the core–cladding interface: first, in that the elements of their cladding have cylindrical symmetry (more precisely, the elements have a nearly circular or elliptical cross section [23]) and, second, in that they can be arranged around the

A.V. Gladyshev, A.N. Kolyadin, A.F. Kosolapov, Yu.P. Yatsenko, A.D. Pryamikov, E.M. Dianov Fiber Optics Research Center, Russian Academy of Sciences, ul. Vavilova 38, 119333 Moscow, Russia;
A.S. Biriukov, I.A. Bufetov Fiber Optics Research Center, Russian Academy of Sciences, ul. Vavilova 38, 119333 Moscow, Russia; Moscow Institute of Physics and Technology (State University), Institutskii per. 9, 141700 Dolgoprudnyi, Moscow region, Russia; e-mail: iabuf@fo.gpi.ru

Received 15 June 2015; revision received 17 July 2015
Kvantovaya Elektronika **45** (9) 807–812 (2015)
Translated by O.M. Tsarev

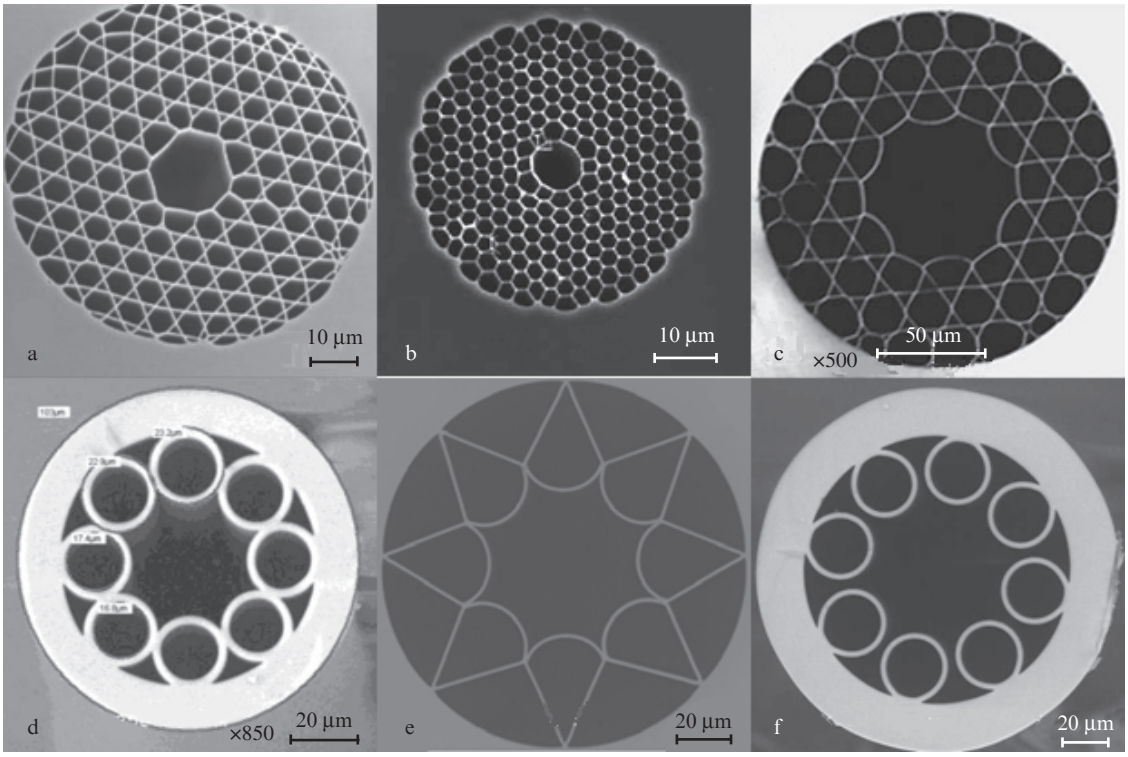

Figure 1. Cross-sectional electron-microscopic images of various types of hollow-core optical fibres: (a) Kagome lattice PCF [14]; (b) PCF with a hexagonal cladding structure [16]; (c) Kagome lattice PCF with a hypocycloid-shaped core–cladding interface [20]; (d) revolver-type HC fibre with contacting capillaries [21]; (e) HC fibre with parachute-shaped cladding elements; (f) revolver-type HC fibre with noncontacting capillaries (this work; configuration first examined by Kolyadin et al. [24]).

core without contacting each other, which allows fibre characteristics to be improved [24, 25] (Fig. 1f). It is, therefore, reasonable to use special notation for fibres of the type represented in Figs 1d and 1f. Since their cross section resembles that of a revolver cylinder, they will be referred to as 'revolver-type' HC fibres.

In this paper, we report the first efficient IR Raman source at $\lambda_S = 1.9$ μm based on a revolver-type fibre with a hydrogen-filled hollow core. In contrast to a previous study [18], we use steady-state Raman conversion due to comparatively long pump pulses ($\tau = 125$ ns). We have studied the spectral and temporal characteristics of the Raman laser and measured its SRS threshold as a function of molecular hydrogen pressure in the HC fibre.

2. Experimental setup

The cross section of the revolver-type HC fibre developed for this study is shown in Fig. 1f. Its outer diameter is 155 μm. The fibre is made of Heraeus F-300 pure silica glass. The air core of the fibre is formed by eight capillaries with a wall thickness of 2.35 μm and outer diameter of 28.7 μm. The air core diameter is 57 μm and the calculated fundamental mode diameter at the pump wavelength is 40.4 μm. The optical loss spectrum obtained for this fibre by numerical simulation has the form of several transmission bands separated by high-loss bands [Fig. 2, spectrum (*1*)]. An important point is that the pump wavelength ($\lambda_p = 1.064$ μm) and first Stokes wavelength ($\lambda_S = 1.907$ nm) lie in the region of optical loss minima in the corresponding transmission bands. Note also that the wavelengths of a number of anti-Stokes components also fall in the low optical loss region (Fig. 2).

Also shown in Fig. 2 is the experimentally measured loss in the revolver-type HC fibre at wavelengths from 1 to 2 μm [spectrum (*2*)]. The calculated and experimentally determined

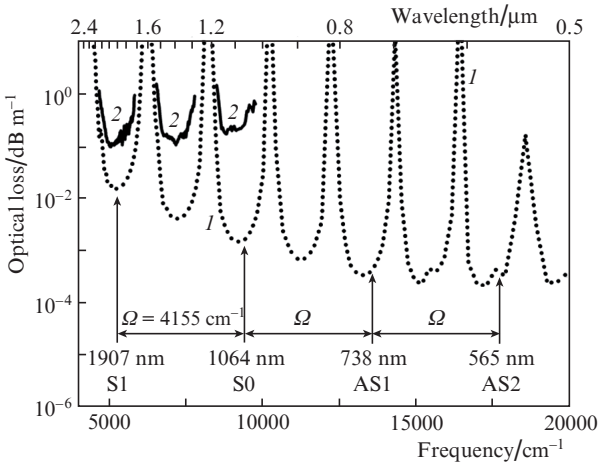

Figure 2. (*1*) Calculated and (*2*) measured optical loss spectra for the fundamental mode of the revolver-type HC fibre. The vertical arrows indicate the pump wavelength (S0) and the spectral position of one vibrational Stokes component (S1) and two vibrational anti-Stokes components (AS1, AS2); $\Omega = 4155$ cm^{-1} is the shift corresponding to the Q(1) vibrational transition of molecular hydrogen.

spectral positions of the transmission bands agree well, whereas the measured optical loss significantly exceeds the calculated one. The discrepancy is probably caused by two factors: deviations of the real fibre structure from the ideal parameters (used in our calculations) and uncertainties in our optical loss measurements for the fundamental mode of the HC fibre, arising from uncontrolled excitation of higher order modes (which have considerably higher losses) in the measurement process. Since the number of modes supported by the fibre increases with increasing frequency, the contribution of the higher order modes to the measured optical loss causes the observed minimum loss to increase in going to higher frequency transmission bands. The measured optical loss at the pump wavelength (1064 nm) and first Stokes wavelength (1907 nm) was 0.25 and 0.1 dB m^{-1}, respectively.

Figure 3 shows a schematic diagram of the experiment. The pump source used was a Q-switched solid-state Nd:YAG laser emitting at 1064 nm. The laser generated 125-ns pulses at a repetition rate of 1.2 kHz and an average power of up to 4 W. With a total emission bandwidth of 0.07 ± 0.01 nm, the laser output was single-mode and elliptically polarised. To control the power level and polarisation state of the laser beam, it was passed through a Glan prism (GP1) to give a linearly polarised beam. Next, the linearly polarised light was sequentially passed through a $\lambda/2$ plate and another Glan prism (GP2), which allowed us to gradually vary the beam power by rotating the $\lambda/2$ plate. The polarisation state of the transmitted beam was controlled using a $\lambda/4$ plate.

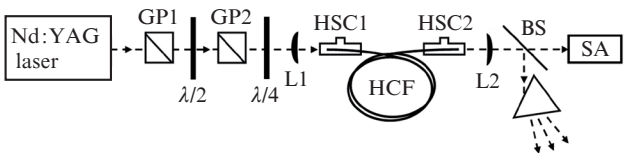

Figure 3. Schematic of the experimental setup: (GP1, GP2) Glan prisms; ($\lambda/2$, $\lambda/4$) half- and quarter-wave plates for 1064 nm; (L1, L2) lenses; (HSC) hermetically sealed miniature cell; (HCF) hollow-core fibre; (BS) beam splitter; (SA) spectrum analyser.

The beam was coupled into the revolver-type HC fibre using a plano-convex lens (L1) with a focal length of 60 mm, which ensured ~53 % coupling efficiency. The fibre length in our experiments was 2.25 m. The fibre ends were secured in hermetically sealed miniature cells (HSCs), which had a sapphire window for light incoupling and outcoupling. The gas delivery system allowed the cells and fibre to be filled with molecular hydrogen at pressures in the range 1 – 31 atm at room temperature. At the fibre output, the beam was collimated by a micro-objective (L2) and directed to a beam splitter. After the beam splitter, one optical channel was used for spectral measurements with different types of spectrum analysers, which ensured a sensitivity range from 200 to 2400 nm. The other component of the beam was passed through a dispersion prism. Next, the power of individual spectral components was determined by a power meter. To determine the shape of pump and first Stokes pulses, a photodetector with a 6-ns time resolution was used instead of the power meter. The photodetector signal was visualised using a high-speed 1-GHz oscilloscope. Placing a white paper sheet instead of the power meter, we were able to obtain the visible emission spectrum at the fibre output using a conventional camera (Fig. 4b).

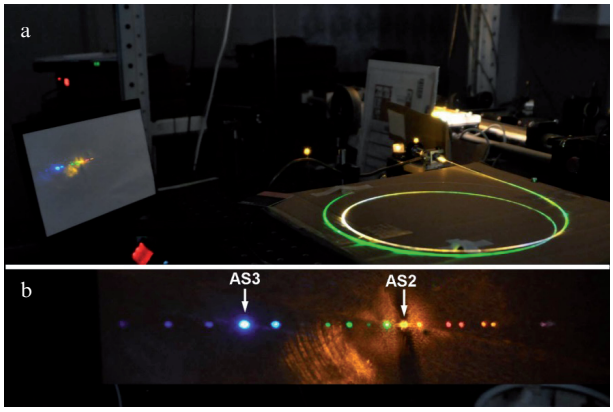

Figure 4. (a) General view of emission from the revolver-type HC fibre at p = 31 atm and a pump power above the threshold for Stokes generation at a wavelength of 1.907 μm; (b) output visible emission spectrum obtained after the dispersion prism under the same conditions as above. The high brightness of the AS2 (565 nm) line prevented us from measuring the spectrum in a wide wavelength range, so it was reduced using a specially designed mask placed between the prism and screen. The colours are somewhat distorted because of the specific features of the spectral sensitivity of the camera.

3. Results and discussion

When the pump power in the HC fibre at a hydrogen pressure of 31 atm exceeded some threshold (P_{th}), we observed Stokes generation at 1907 nm. In addition, there was a considerable number of anti-Stokes components in the range from the UV to λ_p (Fig. 4). The Stokes and anti-Stokes components propagated only in the pump propagation direction, and the observed radial intensity distribution in all the Stokes and anti-Stokes components roughly corresponded to the fundamental mode. The overall anti-Stokes power did not exceed 2% of the power of the first Stokes (1907 nm) component. The spectral position of the components corresponded to a change in pump photon energy by various linear combinations of the energies of vibrational [Q(1)] and rotational [S(1)] transitions of ortho-hydrogen [18, 26]. At a high gas pressure (31 atm in this study), the Raman gain coefficient reaches a maximum level and is independent of pressure [27]. Under such conditions, the SRS threshold for the vibrational transition of molecular hydrogen was reached at an average launched pump power of ~300 mW.

Figure 5 shows a characteristic scattered visible light spectrum observed through the lateral surface of the revolver-type HC fibre (see Fig. 4a). The strongest lines are observed at 738, 565, 457 and 384 nm. These wavelengths correspond to four anti-Stokes components (AS1 – AS4) of the Q(1) vibrational Raman transition in molecular hydrogen. In addition, the spectrum contains a number of weaker lines, some of which (e.g. those at 830 and 880 nm) arise from the xenon lamp used to pump the neodymium laser and the others correspond to scattering from the vibrational transition of ortho-hydrogen with a Stokes shift ω = 587 cm^{-1}.

Emission spectra obtained at the output end of the revolver-type HC fibre are presented in Fig. 6 in a wide spectral range, which includes both the visible and IR spectral

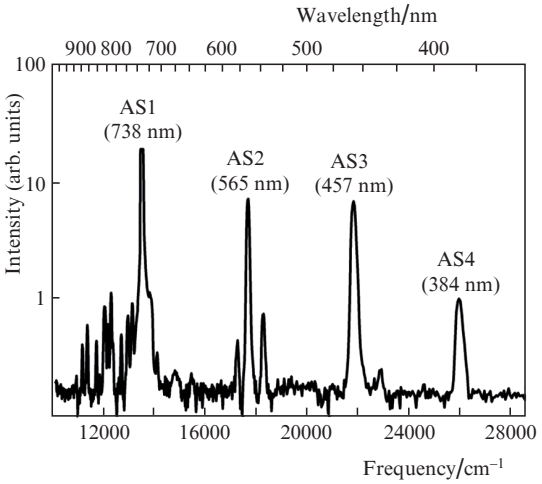

Figure 5. Visible emission spectrum observed through the lateral surface of the revolver-type HC fibre; $p = 31$ atm.

regions. Spectra (*1*) in Fig. 6 were obtained with linearly polarised pump light. In addition to the pump wavelength (1064 nm), the spectrum contains the first Stokes line (1907 nm) and the first (738 nm) and second (565 nm) anti-Stokes lines, which result from pump light scattering by the Q(1) vibrational transition of molecular hydrogen, with a frequency shift $\Omega = 4155$ cm^{-1}, and from four-photon interaction of the pump light with the Stokes and anti-Stokes components. It can be seen that the pump conversion to the Stokes wave is the most efficient. When circularly polarised pump light was used, the Raman spectrum contained, in addition, lines shifted by a frequency $\omega = 587$ cm^{-1} [Fig. 6, lines (*2*)] (like in Wang et al. [18]), suggesting that the Raman process involved the S(1) rotational transition. The differences between noise levels and spectral linewidths are caused by the fact that the overall spectrum presented in Fig. 6 was obtained using three spectrometers, which differed in sensitivity and resolving power. It is worth noting

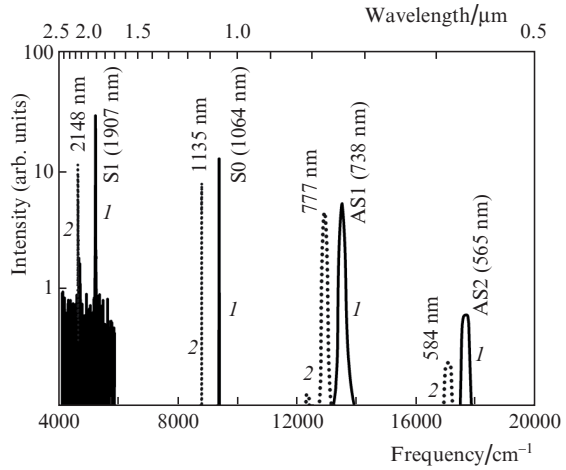

Figure 6. Emission spectra at the output of the molecular hydrogen-filled revolver-type HC fibre at a pump power twice as high as the SRS threshold ($p = 31$ atm). The spectra were measured at (*1*) linear and (*1*, *2*) circular pump beam polarisations.

that the reason for the significantly larger number of spectral components in the spectrum presented in Fig. 4 in comparison with that in Fig. 6 is that the former spectrum was obtained in an experimental configuration without components intended to control the power level and polarisation of the beam (Glan prisms and wave plates), which enabled an about twofold increase in the pump power launched into the HC fibre.

Figure 7 shows the output Stokes power [curve (*1*)] and transmitted pump power [curve (*2*)] as functions of the average pump power launched into the revolver-type HC fibre. The measurements were performed with linearly polarised pump light at a hydrogen pressure of 31 atm. The vibrational SRS threshold P_{th} was reached at an average launched pump power of 0.3 W, which corresponded to a threshold peak power of 2 kW and intensity of 0.16 GW cm^{-2}. The pump (1064 nm) to Stokes (1907 nm) conversion efficiency in our experiments was 33.5%. Because of the large difference in photon energy between the pump light and first Stokes in the case of hydrogen Raman lasers, it is more convenient to specify the fraction of pump photons converted to Stokes photons, i.e. quantum efficiency, which reached 60% in our experiments. We achieved a record high SRS conversion efficiency for a vibrational transition of molecular hydrogen in HC fibres, which exceeds values reported by Wang et al. [18], who obtained 27% power efficiency and 48% quantum efficiency.

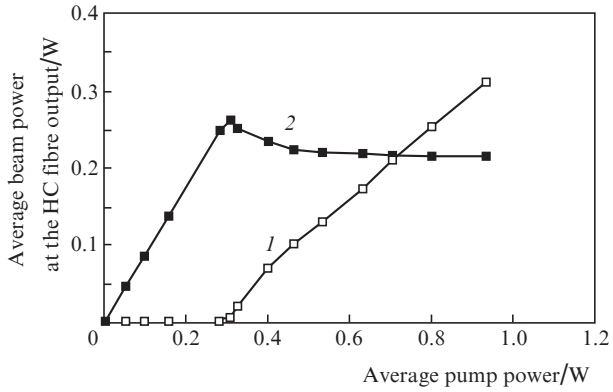

Figure 7. (*1*) Average output Stokes power at $\lambda = 1907$ nm and (*2*) transmitted pump power at $\lambda = 1064$ nm as functions of the average pump power launched into the HC fibre. Fibre length, 2.25 m; hydrogen pressure, 31 atm.

Above the SRS threshold, the output power at the Stokes wavelength is an almost linear function of launched pump power, without any signs of saturation up to the maximum pump power reached (Fig. 7). This strongly suggests that the average output Stokes power of 330 mW (peak power of 3 kW) reached in this study is not a limit. It is also worth noting that, in our experiments, the differential quantum efficiency [corresponds to the linear portion of curve (*1*) in Fig. 7] reached 87%.

Figure 8 demonstrates the shapes of pump and Stokes pulses at the HC fibre output. The Stokes pulse duration (93 ns) is considerably shorter than the pump pulse duration (125 ns). It is also seen that pump powers above the SRS threshold produce a dip in the central part of the pump pulse.

In Fig. 9, the threshold peak pump power for SRS, measured in our experiments as a function of the hydrogen pres-

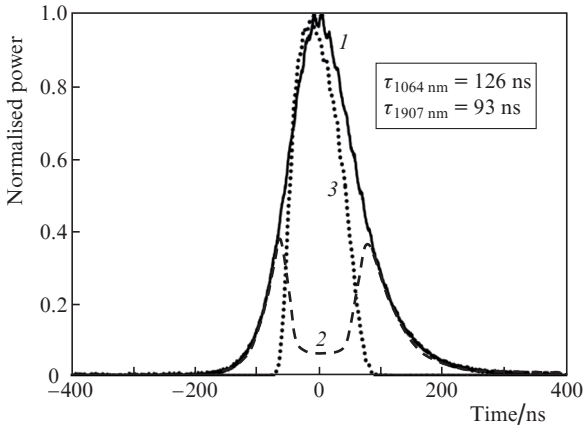

Figure 8. Shapes of pump and Stokes pulses at the output of the hydrogen-filled revolver-type HC fibre: (*1*) pump pulse below the SRS threshold; (*2*) pump and (*3*) Stokes pulses at a pump power a factor of 2.5 above the SRS threshold.

sure in the HC fibre, is represented by data points, and the solid line represents an approximate $P_{th}(p)$ dependence calculated using previous data [27, 28]. It can be seen that there is satisfactory agreement between the experimentally determined and calculated SRS thresholds. At high pressures ($p \geqslant 10$ atm), where the Raman gain bandwidth is determined by collisional broadening, the SRS threshold is independent of hydrogen pressure and has a minimum value: peak pump power of 2 kW.

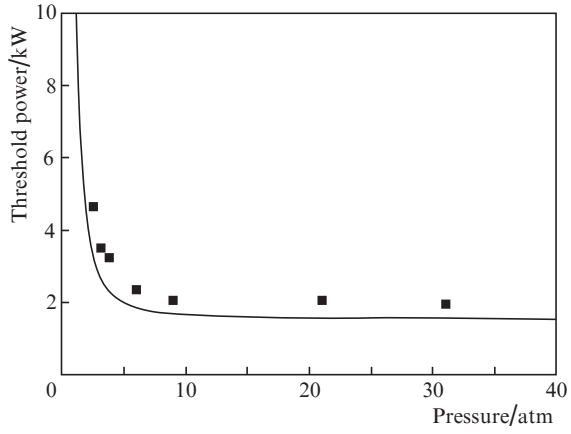

Figure 9. Experimentally determined (data points) and calculated (solid curve) threshold power for SRS as a function of molecular hydrogen pressure in the HC fibre.

4. Conclusions

We have investigated steady-state (τ = 125 ns) 1.06 μm → 1.9 μm SRS conversion in a specially designed, molecular hydrogen-filled revolver-type hollow-core fibre. The fibre offers low optical losses: 0.25 dB m^{-1} at the pump wavelength (1.06 μm) and 0.1 dB m^{-1} at the first Stokes wavelength (1.9 μm). The SRS threshold as a function of the hydrogen pressure in the core of the revolver-type fibre has been shown to agree well with data available in the literature. At high pressures ($p > 10$ atm), the threshold peak pump power for SRS is 2 kW. The pump-to-Stokes conversion quantum efficiency is 60% (differential quantum efficiency of 87%), exceeding the conversion efficiency in previous studies. The average output Stokes power is 330 mW, corresponding to 3 kW of peak power at a Stokes pulse duration of 93 ns. The output Stokes power does not show any signs of saturation and can be raised by using higher pump powers. The parameters of the 1.9-μm Raman fibre laser obtained in this study demonstrate the feasibility of producing efficient, compact, single-stage Raman gas lasers based on gas-filled hollow-core fibres and operating in the range 1.9–10 μm. Note that, to vary the laser wavelength across this range, it is sufficient to vary the pump wavelength between 1 and 2 μm.

Acknowledgements. This work was supported in part by the Russian Foundation for Basic Research (Grant No. 15-02-08840).

References

1. Dianov E.M. *J. Lightwave Technol.*, **20**, 1457 (2002).
2. Basiev T.T., Osiko V.V., Prokhorov A.M., Dianov E.M. In: *Solid-State Mid-Infrared Laser Sources, Topics Appl. Phys.* (Berlin–Heidelberg: Springer-Verlag, 2003) Vol. 89, p. 351.
3. Minck R.W., Terhune R.W., Rado W.G. *Appl. Phys. Lett.*, **3**, 181 (1963).
4. Grasyuk A.Z., Zubarev I.G., Kotov A.V., Mikhailov S.I., Smirnov V.G. *Kvantovaya Elektron.*, **3**, 1062 (1976) [*Sov. J. Quantum Electron.*, **6**, 568 (1976)].
5. Byer R.L., Trutna W.R. *Opt. Lett.*, **3**, 144 (1978).
6. Tashiro H., Midorikawa K., Aoki Y., Nagasaka K., Toyoda K., Namba S. *Opt. Lett.*, **10**, 80 (1985).
7. Ippen E.P. *Appl. Phys. Lett.*, **16**, 303 (1970).
8. Stolen R.H., Ippen E.P., Tynes A.R. *Appl. Phys. Lett.*, **20**, 62 (1972).
9. Grubb S., Erdogan T., Mizrahi V., Strasser T., Cheung W.Y., Reed W.A., Lemaire P.J., Miller A.E., Kosinski S.G., Nykolak G., Becker P.C. *Proc. Top. Meet. 'Opt. Amplifiers Appl.'* (Breckenridge: 1994) PD3-1, p. 187.
10. Dianov E.M., Grekov M.V., Bufetov I.A., Vasiliev S.A., Medvedkov O.I., Plotnichenko V.G., Koltashev V.V., Belov A.V., Bubnov M.M., Semjonov S.L., Prokhorov A.M. *Electron. Lett.*, **33**, 1542 (1997).
11. Bufetov I.A., Dianov E.M. *Kvantovaya Elektron.*, **30**, 873 (2000) [*Quantum Electron.*, **30**, 873 (2000)].
12. Dianov E.M., Bufetov I.A., Mashinsky V.M., Shubin A.V., Medvedkov O.I., Rakitin A.E., Mel'kumov M.A., Khopin V.F., Gur'yanov A.N. *Kvantovaya Elektron.*, **35**, 435 (2005) [*Quantum Electron.*, **35**, 435 (2005)].
13. Cregan R.F., Mangan B.J., Knight J.C., Birks T.A., Russell P.St.J., Roberts P.J., Allan D.C. *Science*, **285**, 1537 (1999).
14. Benabid F., Knight J.C., Antonopoulos G., Russell P.St.J. *Science*, **298**, 399 (2002).
15. Couny F., Benabid F., Roberts P.J., Light P.S., Raymer M.G. *Science*, **318**, 1118 (2007).
16. Benabid F., Bouwmans G., Knight J.C., Russell P.St.J. *Phys. Rev. Lett.*, **93**, 123903 (2004).
17. Couny F., Benabid F., Light P.S. *Phys. Rev. Lett.*, **99**, 143903 (2007).
18. Wang Z., Yu F., Wadsworth W.J., Knight J.C. *Laser Phys. Lett.*, **11**, 105807 (2014).
19. Wang Y.Y., Couny F., Roberts P.J., Benabid F. *Proc. Conf. Lasers and Electrooptics 2010* (San Jose, Cal., 2010) paper CPDB4.
20. Wang Y.Y., Wheeler N.V., Couny F., Roberts P.J., Benabid F. *Opt. Lett.*, **36**, 669 (2011).
21. Pryamikov A.D., Biriukov A.S., Kosolapov A.F., Plotnichenko V.G., Semjonov S.L., Dianov E.M. *Opt. Express*, **19**, 1441 (2011).
22. Yu F., Wadsworth W.J., Knight J.C. *Opt. Express*, **20**, 11153 (2012).

23. Pryamikov A.D., Biriukov A.S. *Usp. Fiz. Nauk*, **183**, 863 (2013).
24. Kolyadin A.N., Kosolapov A.F., Pryamikov A.D., Biriukov A.S., Plotnichenko V.G., Dianov E.M. *Opt. Express*, **21**, 9514 (2013).
25. Alagashev G.K., Pryamikov A.D., Kosolapov A.F., Kolyadin A.N., Lukovkin A.Yu., Biriukov A.S. *Laser Phys*., **25**, 055101 (2015).
26. Johnson F.M., Duardo J.A., Clark C.L. *Appl. Phys. Lett*., **10**, 157 (1976).
27. Bischel W.K., Dyer M.J. *Phys. Rev. A*, **33**, 3113 (1986).
28. Laubereau A., Kaiser W. *Rev. Mod. Phys*., **50**, 607 (1978).